ELSEVIER

Journal of Nuclear Materials 280 (2000) 18–24

journal of nuclear materials

www.elsevier.nl/locate/jnucmat

Effects of helium on radiation-induced defect microstructure in austenitic stainless steel

E.H. Lee *, J.D. Hunn, T.S. Byun, L.K. Mansur

Metals and Ceramics Division, Oak Ridge National Laboratory, P.O. Box 2008, Oak Ridge, TN 37831-6376, USA

Received 26 January 2000; accepted 7 March 2000

Abstract

In the construction materials surrounding the spallation neutron source (SNS) mercury target, considerable quantities of transmutation products, particularly hydrogen and helium, will be generated due to the exposure to a high flux of 1 GeV protons and associated neutrons. In an effort to investigate the effects of high helium, therefore, bubble formation and defect clustering processes in AISI 316 LN austenitic steel were studied as a function of helium concentration and displacement damage dose with 360 keV He^+ and 3500 keV Fe^+ ion beams at 200°C. Helium irradiation was less effective in producing defects such as black dots and dislocation loops than Fe^+ ion irradiation at equivalent displacement dose. On the other hand, the formation of helium bubbles produced a strong depressive effect on the growth of loops and the evolution of line dislocations. The results indicated that the effect of helium bubbles was augmented as the bubble number density and size increased with increasing helium beyond 1 atomic percent (at.%). In such a case, the effect of helium bubbles can be more important than that of radiation-induced defects on the evolution of microstructure and the change in mechanical properties.

1. Introduction

For future neutron scattering research, the construction of an accelerator based spallation neutron source (SNS) facility, operating at approximately 2 MW, is presently under design and construction [1]. The materials R&D program that is underway for the SNS target includes major efforts on spallation radiation effects [2]. Type AISI 316 austenitic stainless steel is the candidate material for the containment vessel of the mercury (neutron source). The containment vessel will be exposed to an intense pulsed 1 GeV proton beam and to neutrons generated by spallation reactions in the mercury. It is anticipated that atomic displacement rates will be high, up to $\approx 10^{-2}$ dpa/s (displacements per atom/second) during the microsecond beam pulse period, with a 60 Hz pulse frequency. The time average displacement rate would be in the range of $\approx 10^{-6}$ dpa/s. The operating temperature is expected to be below 200°C. Besides the radiation-induced displacement damage, various transmutation products will be generated as a result of nuclear reactions. In particular, hydrogen and helium will be produced at rates of ≈1000 and ≈100 appm/dpa, respectively.

One of the major concerns is the ductility loss of the vessel material due to radiation-induced hardening and helium effects, which could limit the serviceable lifetime of the vessel. In recent work [3], a dramatic increase in hardness was observed in association with bubble formation when helium was implanted to a level of 10 at.%. In our on-going work in parallel to the present study, to be published in a separate paper, it was found that the hardness increase by helium implantation alone began to exceed the saturation hardness value achieved by displacement damage with 3500 keV Fe^+ ions at 1 at.% He level and reached a saturation hardness value which was twice as high as that by Fe ions at 10 at.% He level. However, it is important to note that for the presently anticipated end-of-life dose for the target vessel of SNS (<10 dpa), the helium level would be below 2000 appm. Nonetheless, there is little systematic information to

* Corresponding author. Tel.: +1-865 574 5058; fax: +1-865 574 0641.

E-mail address: leeeh@ornl.gov (E.H. Lee).

0022-3115/00/$ - see front matter
PII: S0022-3115(00)00038-6

evaluate the effects of the high helium to dpa rates expected under the SNS condition. The aim of this work is to study the agglomeration process of helium as a function of helium concentration and its impact on microstructural change in order to provide information to guide design and lifetime estimates for the SNS target vessel.

In this work, AISI 316 LN austenitic stainless steel was irradiated with 360 keV He^+ or 3500 keV Fe^+ ion beams at 200°C with systematic increment in helium concentration and displacement dose. Microstructural evolution during helium irradiation was studied by comparing with the displacement induced defect microstructure by Fe^+ ions.

2. Experimental

A solution annealed AISI 316LN stainless steel (Jessop Steel Company Heat # 18474) was used for this investigation. The nominal composition of the alloy was, in weight percent, 16.3 Cr, 10.2 Ni, 2.01 Mo, 1.75 Mn, 0.39 Si, 0.009 C, 0.11 N, 0.029 P with the balance Fe. Disks of 3 mm diameter and 0.25 mm thickness were prepared by mechanical and electrochemical polishing prior to irradiation. Irradiation was carried out at 200°C with 360 keV He^+ or 3500 keV Fe^+ ion beams using the triple ion facility (TIF) at ORNL. Details of the TIF can be found in [4]. The ion energies were chosen for the maximum gas atom deposition and damage to occur near a depth of 750–850 nm. For the depth calculations, the computer code, Stopping and Range of Ions in Matter (SRIM, 1998 version) was used [5]. The procedure for the dpa calculation is described in [6]. The He^+ ion beam was applied with a deposition rate of $\simeq 0.2$ appm/s at the peak, which also produced a displacement damage at a rate of $\simeq 7.5 \times 10^{-5}$ dpa/appm or $\simeq 1.5 \times 10^{-5}$ dpa/s. This gives the helium appm/dpa ratio almost 100 times higher than that expected in the actual SNS target. The implanted helium concentration levels were from 2 appm (2×10^{-4} at.%) to 500 000 appm (50 at.%) and the corresponding doses were from $\simeq 1.5 \times 10^{-4}$ to $\simeq 37$ dpa. To appraise the damage microstructure produced by helium, a set of reference irradiation was carried out separately with 3500 keV Fe^+ ions at a rate of $2–3 \times 10^{16}$ ions/m^2/s ($\simeq 1 \times 10^{-3}$ dpa/s at the peak).

Transmission electron microscopy (TEM) specimens were prepared by electrochemically removing $\simeq 700$ nm from the ion bombarded side of the disks and then thinning from the unirradiated side until perforation occurred. This procedure produced TEM foils with thicknesses of $\simeq 100$ nm on average and allowed examination of the microstructure at the peak damage region between 700 and 800 nm original depth. Damage microstructure was examined with a Philips CM12 electron microscope operated at 120 keV.

3. Results

The bubbles and defect clusters were examined after helium irradiation to various concentration levels. At low helium concentration levels ($\lesssim 2$ at.%), it was very difficult to image bubbles clearly by TEM because bubbles were too small in size ($r < 0.2$ nm) and too high in number density. However, the grainy microstructure revealed increasingly bubble-like features with increasing helium concentration in high magnification micrographs. Discernible bubbles could be imaged at a helium level of 5 at.% ($\sim 1.5 \times 10^{23}$ He/m^2). Patches of a well-defined lattice of bubbles were visible at 5 at.% helium level as indicated in the magnified inset of Fig. 1, although complete bubble alignment was not observed as found in 30 keV He^+ ion irradiated copper elsewhere [7]. The bubble lattice spacing was in the range of 1.5 ± 0.3 nm, the bubble radii were smaller than 0.3 nm, and the bubble number density was estimated to be in the range $2–6 \times 10^{26}$ m^{-3}. With increasing helium concentration, bubbles assumed a more distinctive spherical shape, but bubble coalescence was insignificant up to 10 at.% helium. A significant fraction of bubbles coalesced at 20 at.% helium as shown in Fig. 2 and a severe blistering occurred at the irradiated surface at 50 at.%. Although the blistering might have caused some variation in dose from area to area, the larger and coarser bubble microstructure in the 50 at.% He-implanted specimen indicated that the examined area appeared to be an area not affected by the blistering.

As already mentioned, helium implantation also produced atomic displacement damage at a rate of $\simeq 7.5 \times 10^{-5}$ dpa/appm. Black dots (vacancy and interstitial clusters) and Frank type faulted interstitial loops evolved on {1 1 1} planes with increasing helium concentration. It is known that most surviving defect clusters are interstitial clusters [8,9]. Fig. 3 illustrates defect microstructures for 0.02, 0.2, 2, and 10 at.% helium, which also produced 0.015, 0.15, 1.5 and 7.5 dpa damage, respectively. Very few defects were visible at 0.02 at.% (0.015 dpa). At 0.2 at.% (0.15 dpa), a high number density of black dots evolved but were too small to produce good images within the TEM resolution limit. At 2 at.% (1.5 dpa), black dots were small ($\lesssim 1$ nm) but the number density approached a saturation level and occasional small loops began to develop. The number density of black dots and loops was estimated to be in the range $2–4 \times 10^{23}$ m^{-3} from high magnification micrographs. We use the term loops when defect clusters become large (>5 nm) and take on a planar disk morphology. With increasing helium fluence, some black dots were converted to Frank type interstitial faulted loops as they grew but there was very little indication of unfaulting to prismatic loops even at 50 at.%. Loop growth was noticeably suppressed during He^+

irradiation compared to that of Fe^+ irradiation, as described below.

Although a similar defect evolution occurred during 3500 keV Fe^+ ion irradiation, black dot formation and loop growth occurred at somewhat lower dose in Fe^+ irradiation than in He^+ irradiation. Neither bubbles nor cavities were observed after Fe^+ irradiation. Fig. 4 illustrates the defect microstructure after

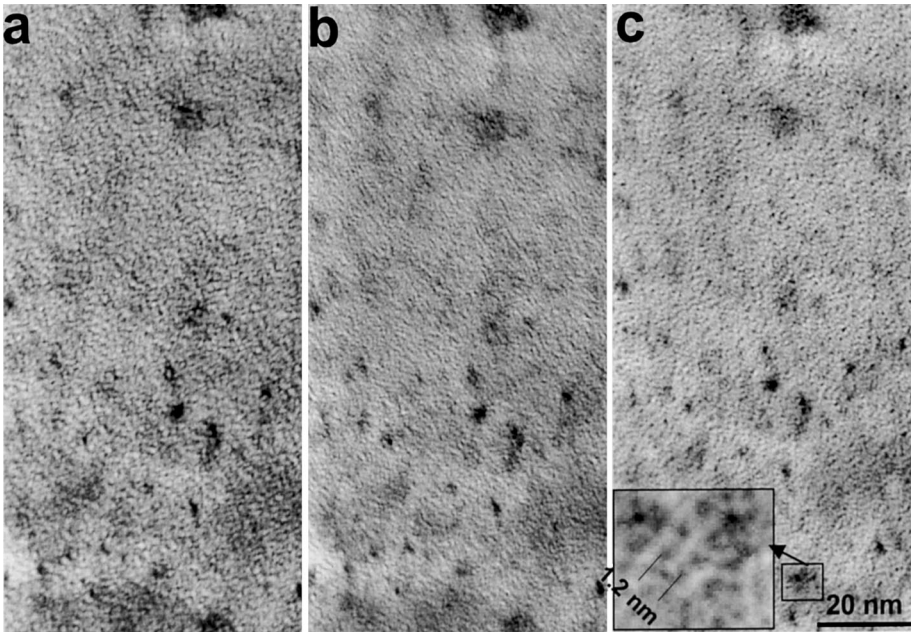

Fig. 1. Bubble microstructure after 5 at.% helium implantation with 360 keV He^+ ions at 200°C. The micrographs are taken near $Z = [1\,1\,0]$: (a) under-focus, (b) near-focus, and (c) over-focus images. The magnified inset shows an area of aligned bubbles in which the spacing between the bubble lattices is found to be in the range of 1.5 ± 0.3 nm and the bubble number density is estimated to be in the range of $2–6 \times 10^{26}$ m^{-3}.

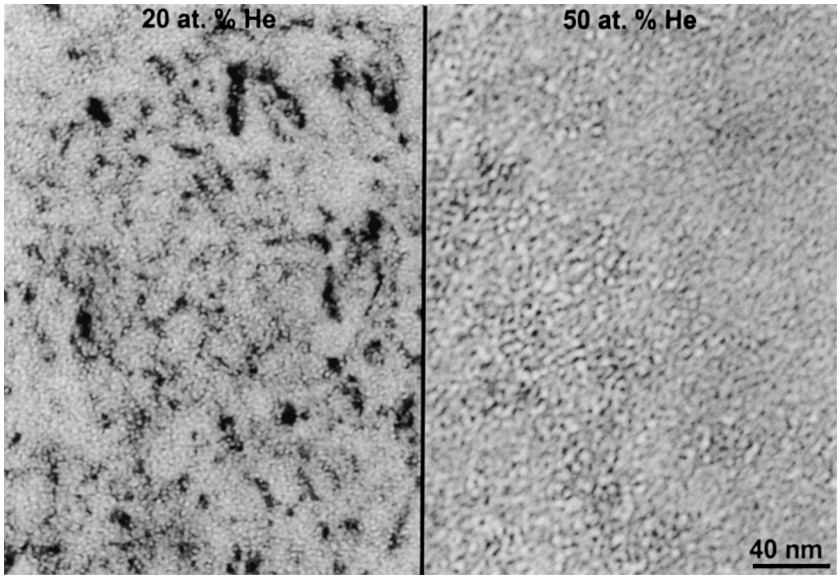

Fig. 2. Bubble microstructure after (a) 20 and (b) 50 at.% helium implantation with 360 keV He^+ ions at 200°C. A significant fraction of bubbles coalesced at 20 at.% and a severe blistering occurred on the irradiated surface at 50 at.%.

0.01, 0.1, 1, and 10 dpa Fe^+ ion irradiation. At 0.01 dpa, defects were not visible. At 0.1 dpa, black dots were well established and some small loops began to evolve. At 1 dpa, small but copious well-defined loops were visible. At 10 dpa, some large faulted loops began to unfault to prismatic loops. The black dot and loop number density appeared to saturate between 0.1 and 1 dpa. Here, it should be pointed out that the image of a small loop or black dot comes from the strain-field around the cluster and varies strongly with Bragg diffracting condition, so it is often difficult to make a precise size determination from a TEM image; the defect cluster sizes at 0.1 dpa appeared to be larger than at a dose of 1 dpa because of the difference in diffracting conditions and partly due to streaking.

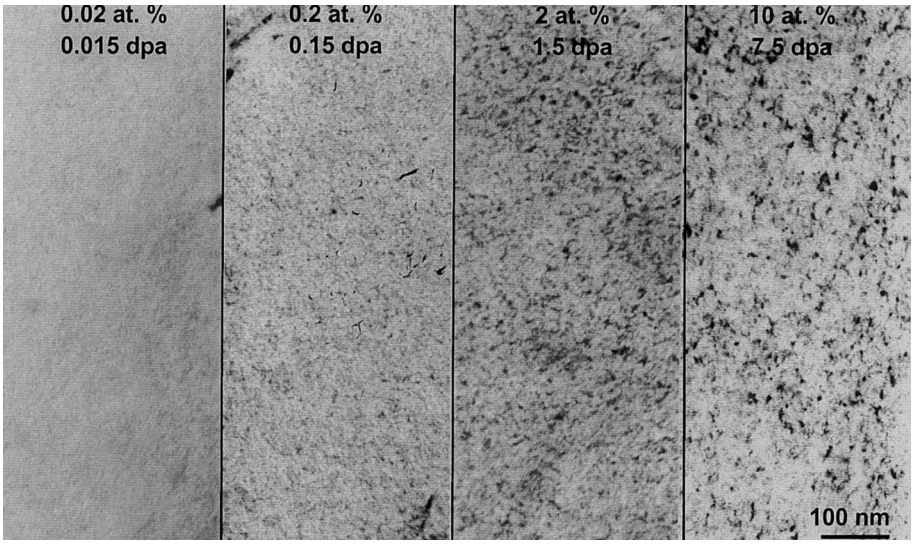

Fig. 3. Defect microstructure after 0.02, 0.2, 2, and 10 at.% (or 0.015, 0.15, 1.5, and 7.5 dpa) irradiation with 360 keV He^+ ions at 200°C.

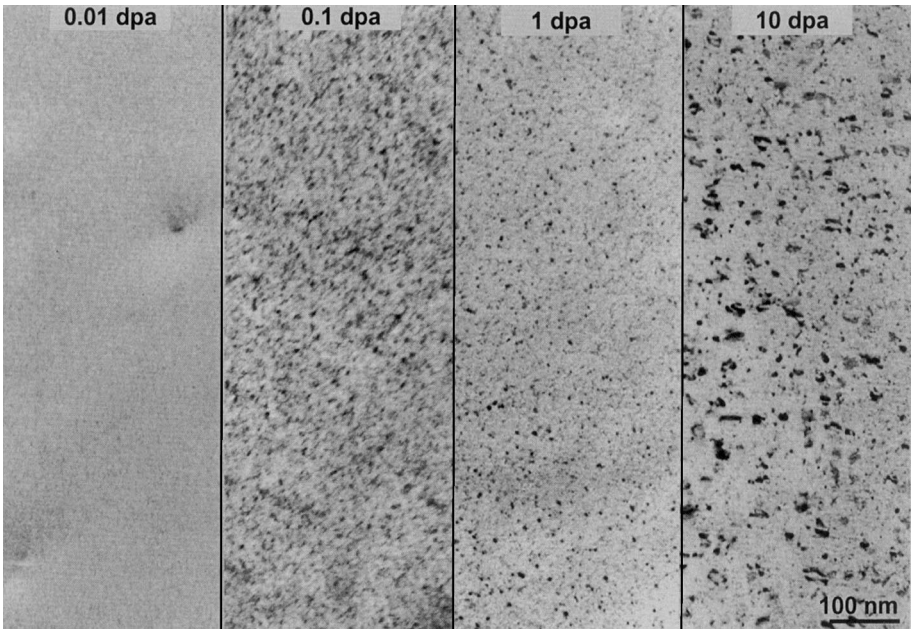

Fig. 4. Defect microstructure after 0.01, 0.1, 1, and 10 dpa irradiation with 3500 keV Fe^+ ions at 200°C.

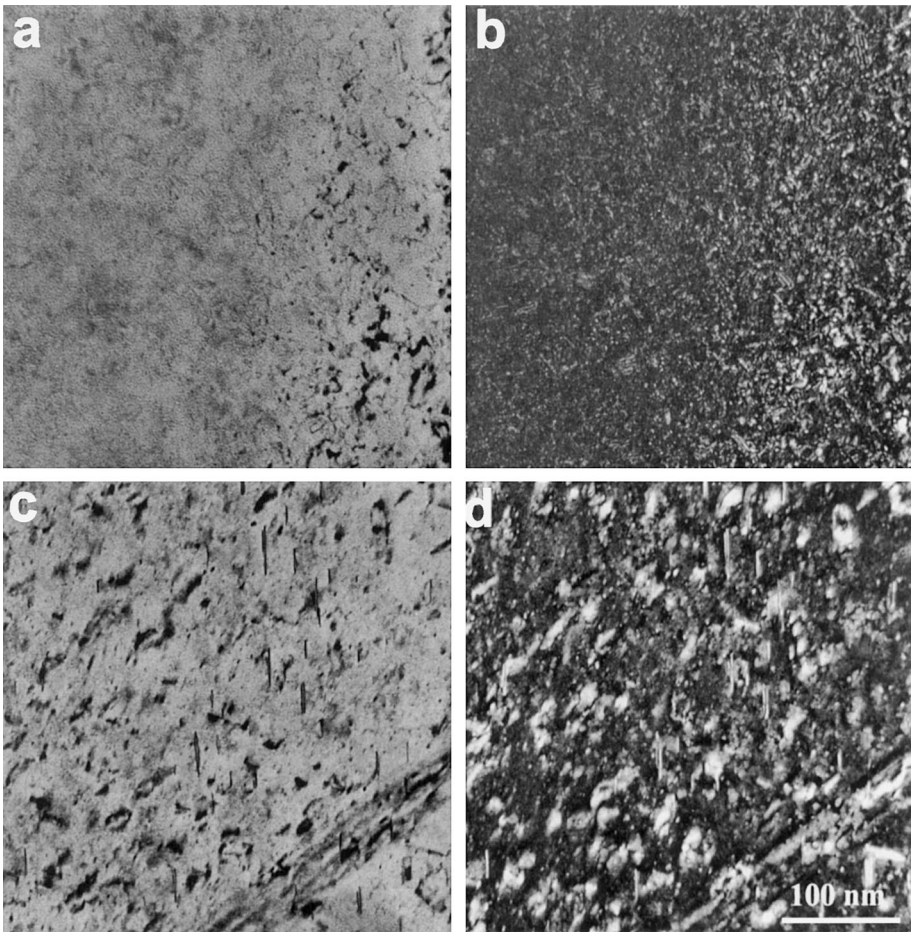

Fig. 5. Bright and dark field defect microstructure (a) and (b) after 50 at.% (37 dpa) He implantation, and (c) and (d) after10 dpa Fe^+ irradiation. Black dot and loop sizes in (a) and (b) are smaller despite the higher displacement damage dose.

Under He^+ irradiation, not only black dots evolved slowly but also loop growth was suppressed noticeably. Fig. 5 compares the defect microstructures for 50 at.% (37 dpa) He versus 10 dpa Fe. The defect clusters in the He-implanted specimen were noticeably smaller than those in the Fe irradiated one, even though the displacement dose for He was almost four times higher.

4. Discussion

As described in Section 2, the microstructures in the depth between 700 and 800 nm depth were examined after removing about 700 nm surface region. A calculation based on a rate theory model showed that point defects at this depth would not see the free surface effect, particularly at low temperature and high sink density conditions where most point defects were recombined or captured by sinks before any significant diffusion could occur [10]. Thus, the microstructures in the depth examined here were considered to represent the bulk behavior. The most notable observation was that the black dot evolution and loop growth was slower for He irradiation compared with Fe irradiation at equivalent dpa dose. The suppressed defect evolution is attributable to the lower displacement damage rate for He irradiation, smaller cascade energies produced by a lower mass and lower energy He^+ ion, enhanced point defect recombination at helium bubbles, and dislocation pinning by bubbles. These effects are described further below.

During irradiation, vacancies and interstitials are generated as a result of displacement damage. Some of these point defects are absorbed by pre-existing or generated defects such as dislocations, grain boundaries, precipitates, and cavities, and the rest are either annihilated via direct recombination or form clusters. At a given temperature, the point defect supersaturation decreases with decreasing damage rate, but the fraction of surviving point defects is higher at a lower damage rate, since the probability of point defect recombination is

lowered in proportion to the product of vacancy and interstitial concentration, which are lower at lower displacement rate [11]. However, the nucleation rate of defect clusters is lower at lower damage rate because the absolute point defect flux to sinks is lower. The employed He^+ ion energy (360 keV) was about 10 times lower than that of the Fe^+ ion (3500 keV) and the damage rate from He^+ ($\simeq 1.5 \times 10^{-5}$ dpa/s) was about two orders of magnitude lower than that from Fe^+ ($\simeq 1 \times 10^{-3}$ dpa/s). A slower defect-clustering rate is thus expected for He^+ ion irradiation because of the lower damage rate.

The second reason for the slower defect nucleation rate in He^+ irradiation is due to the smaller cascade energy of He^+ ions because of the lower ion mass and energy. When an ion penetrates into a material, the incident ion energy is transferred to the target atoms via nuclear and electronic energy loss processes. Atoms displaced from their lattice sites by elastic collisions with the ion are called primary knock-on atoms (PKAs). The PKAs have various energies depending upon the energy received from the ion. PKA energies are similarly transferred to other target atoms in subsequent secondary knock-on processes. The PKAs produced by an ion can be simulated in a full cascade SRIM calculation [5]. A 360 keV He^+ ion produces about 35 PKAs with energy between 40×10^3 and 5.2×10^3 eV, and a 3500 keV Fe^+ ion produces about 350 PKAs with energy between 40×10^6 and 1.6×10^6 eV. Fe^+ ions produce more and higher energy PKAs. About 40% of the PKA energy lies below 100 eV for both ions. Since an average displacement threshold energy for stainless steel is about 40 eV [12], the interstitial clustering for PKA energies below 100 eV is inconsequential within the damage rate range of interest. The value 40 eV was used for all SRIM simulations in this work. In a recent molecular dynamic (MD) simulations of cascade process in bcc iron [9], it was shown that the total number of surviving point defects and the resulting fraction of interstitials in clusters in a cascade increased with increasing cascade energy. Although the austenitic stainless steel studied in this work has a fcc crystal structure, for 3500 keV Fe^+ ion irradiation, a larger number of interstitial clusters per dpa is expected to form because of the larger PKA energy.

In a previous study, we found that defect evolution and void growth were suppressed by a high helium injection rate or in the presence of high bubble number density because of enhanced point defect recombination at bubble sinks [13,14]. Since bubbles were nucleated in high number during the 360 keV He^+ irradiation, point defect recombination at bubble sinks may be an important factor for the slow evolution of black dots and loops. An impeded loop growth has also been observed in the presence of high helium because of pinning by helium bubbles [15]. On the other hand, there is evidence that helium often promotes loop formation by retaining vacancies during the process of helium-vacancy clustering and by punching-out interstitials by over-pressurized helium bubbles [16,17]. In the present study, the relative importance between these two competing effects could not be differentiated. Nevertheless, the microstructural evidence indicated that bubble pinning and enhanced point defect recombination played important roles in loop growth because most loops remained small and faulted in the presence of high helium contents.

A notable finding was that very limited loop growth and unfaulting occurred even at 50 at.% (37 dpa) helium, even though the defect cluster number density saturated near 2 at.% (1.5 dpa). In fact, very little change in microstructure occurred beyond the saturation dose except bubble growth. The primary reason for this static defect microstructure is believed to be due to helium bubbles acting as a barrier to loop growth in addition to enhancing point defect recombination. Helium bubbles are considered to be a weak barrier for dislocation motion [18]. Up to now, there has been no information regarding the synergistic effect of bubble size and number density. However, hardness measurement data reported in other work [3] indicated that, when helium bubbles were present in such high concentration, the barrier strength (hardness) was augmented as bubbles grew, particularly when helium clusters began to become identifiable as bubbles under TEM. That is, at a helium level of above 1 at.%. This trend of microstructural evolution confirms the trend of hardness data measured for the 25 MeV helium implanted 316 L stainless steel by other investigators [3,19] and gives insight into the cause of the high hardness values measured in our more recent work.

5. Conclusions

To investigate the impact of high helium concentrations on a spallation neutron source target material, the microstructural evolution in an AISI 316LN stainless steel was studied after irradiation with 360 keV He^+ and 3500 keV Fe^+ ions. The results indicated that defects (black dots and loops) evolved slower in 360 keV He^+ irradiation than in 3500 keV Fe^+ ion irradiation when the defect microstructure was compared at equivalent damage doses. With increasing helium concentrations above 1 at.%, bubbles grew continuously but loop growth was severely impeded. The slower evolution and growth of defect clusters during 360 keV He^+ irradiation was attributed to the lower damage rate, smaller PKA energies, enhanced point defect recombination at bubble sinks, and dislocation pinning by helium bubbles. An important realization is that barrier strength of helium bubbles increase with increasing bubble size, and that helium bubbles impede not only the motion of disloca-

tions but also the evolution of loops and dislocations. Such effects can augment the radiation-induced hardening and ductility loss for steels subjected to a high helium generation environment. However, within the expected service period of the SNS target, hardening by helium appears to be insignificant.

Acknowledgements

This research was sponsored by the Division of Materials Sciences, US Department of Energy, under contract no. DE-AC05-96OR22464 with Lockheed Martin Energy Research Corporation. The authors thank Drs K. Farrell and Roger E. Stoller for reviewing the paper.

References

[1] Spallation Neutron Source Design Manual, ORNL Report, September 1998.
[2] L.K. Mansur, Trans. ANS, TANSAO 80 (1999) 94.
[3] E. Camus, in: Proceedings of the Second International Workshop on Spallation Materials Technology, Ancona, Italy, 19–22 September 1997, p. 445.
[4] M.B. Lewis, W.R. Allen, R.A. Buhl, N.H. Packan, S.W. Cook, L.K. Mansur, Nucl. Instrum. and Meth. B 43 (1989) 243.
[5] J.F. Ziegler, J.P. Biersack, U. Littmark, The Stopping and Range of Ions in Solids, Pergamon, Oxford, 1985.
[6] E.H. Lee, Nucl. Instrum. and Meth. B 151 (1999) 29.
[7] P.B. Johnson, D.J. Mazey, Radiat. Eff. 53 (1980) 195.
[8] M. Horiki, M. Kiritani, J. Nucl. Mater. 212–215 (1994) 246.
[9] R.E. Stoller, J. Nucl. Mater. 276 (1999) 22.
[10] L.K. Mansur, H.M. Yoo, J. Nucl. Mater. 85&86 (1997) 523.
[11] L.K. Mansur, in: G.R. Freeman (Ed.), Kinetics of Nonhomogeneous Processes, Wiley, New York, 1987, p. 377 (Chapter 8).
[12] ASTM E521, Standard Practice for Neutron Radiation Damage Simulation by Charged-Particle Irradiation, Annual Book of ASTM Standards, vol. 12.02, American Society of Testing and Materials, Philadelphia, PA.
[13] E.H. Lee, L.K. Mansur, Metall. Trans. A 21 (1990) 1021.
[14] E.H. Lee, L.K. Mansur, Metall. Trans. A 23 (1992) 1977.
[15] E.H. Lee, N.H. Packan, M.B. Lewis, L.K. Mansur, Nucl. Mater. Meth. B 16 (1986) 25.
[16] K. Farrell, R.W. Chickering, L.K. Mansur, Philos. Mag. A 53 (1986) 1.
[17] H. Trinkaus, Radiat. Eff. 78 (1983) 189.
[18] S.M. Bruemmer, J.I. Cole, R.D. Carter, G.S. Was, Mater. Res. Soc. Symp. Proc. 439 (1997) 437.
[19] H. Ulmaier, E. Camus, J. Nucl. Mater. 251 (1997) 262.